University of Nebraska - Lincoln
DigitalCommons@University of Nebraska - Lincoln

Roger Kirby Publications

Research Papers in Physics and Astronomy

February 1981

Raman investigation of the charge-density-wave mixed-crystal system 1T-$TaS_{2-x}Se_x$

J.R. Duffey
University of Nebraska-Lincoln

Roger D. Kirby
University of Nebraska-Lincoln, rkirby1@unl.edu

Follow this and additional works at: https://digitalcommons.unl.edu/physics_kirby

 Part of the Physics Commons

Duffey, J.R. and Kirby, Roger D., "Raman investigation of the charge-density-wave mixed-crystal system 1T-$TaS_{2-x}Se_x$" (1981). *Roger Kirby Publications*. 26.
https://digitalcommons.unl.edu/physics_kirby/26

This Article is brought to you for free and open access by the Research Papers in Physics and Astronomy at DigitalCommons@University of Nebraska - Lincoln. It has been accepted for inclusion in Roger Kirby Publications by an authorized administrator of DigitalCommons@University of Nebraska - Lincoln.

PHYSICAL REVIEW B VOLUME 23, NUMBER 4 15 FEBRUARY 1981

Raman investigation of the charge-density-wave mixed-crystal system $1T$-$TaS_{2-x}Se_x$

J. R. Duffey* and R. D. Kirby
Behlen Laboratory of Physics, University of Nebraska, Lincoln, Nebraska 68588
(Received 29 September 1980)

The results of Raman scattering measurements on the mixed-crystal system $1T$-$TaS_{2-x}Se_x$ in the commensurate charge-density-wave state are reported. In the pure compounds, our measurements indicate that a strong LA-TA phonon interaction at the distortion wave-vector results in additional coupled charge-density-wave–lattice excitations. These excitations can be followed over the whole range of concentrations in the mixed crystals. The concentration dependences of the mode frequencies are treated using an effective oscillator model.

I. INTRODUCTION

The $1T$ polytypes of TaS_2 and $TaSe_2$ have been extensively investigated because they exhibit structural phase transitions associated with the formation of charge-density waves, as discussed by Wilson, Di Salvo, and Mahajan.[1] Diffraction measurements by Wilson *et al.*,[1] Scruby *et al.*,[2] and Moncton *et al.*[3] have shown that complex superlattices exist in both compounds. An incommensurate charge-density wave (CDW) exists in $TaSe_2$ above 473 K, with the associated periodic-lattice distortion being described by three symmetry-related distortion wave vectors. In a first-order transition at 473 K, the CDW rotates by 13.9° and becomes commensurate with the crystalline lattice. In this phase, the unit cell of the crystal has dimensions $\sqrt{13}\,a_0 \times \sqrt{13}\,a_0 \times c_0$, where a_0 and c_0 are the lattice constants of the $1T$ structure. $1T$-TaS_2 shows an essentially identical low-temperature commensurate phase and a similar high-temperature phase, but it also has an additional intermediate incommensurate phase between 200 and 350 K. Wertheim, Di Salvo, and Chiang[4] found that the CDW amplitude is approximately one electron per Ta atom, which is consistent with the large ionic displacements (> 0.1 Å) observed by Scruby *et al.*[2]

The diffraction measurements discussed above show that for both compounds the structure of the low-temperature commensurate phase is triclinic with 39 atoms per unit cell. Raman measurements on TaS_2 and $TaSe_2$ in the commensurate CDW phases by Smith, Tsang, and Shafer,[5,6] by Duffey, Kirby, and Coleman,[7] and by Holy[8] show a large number of Raman peaks, as would be expected for such a complex crystalline structure. Infrared measurements by Karecki and Clayman[9] show similar results. Duffey *et al.*[7] attributed some of the observed modes to strongly coupled CDW-lattice excitations because of their large Raman intensities and rapid temperature dependences.

DiSalvo *et al.*[10] have carried out a comprehensive investigation of the effects of anion and cation doping on the electronic and CDW properties of $1T$-TaS_2 and $1T$-$TaSe_2$. In particular, they used resistivity, magnetic susceptibility, and electron diffraction measurements to study the commensurate CDW phase in mixed crystals of TaS_2 and $TaSe_2$. They found that the commensurate CDW state exists in $1T$-$TaS_{2-x}Se_x$ throughout the entire range of concentrations ($0 \leq x \leq 2$) for temperatures below about 120 K. This suggests that the gross properties of the commensurate CDW phase are essentially independent of concentration. The question remains as to what extent anion doping affects the details of the CDW-lattice interaction. This aspect of CDW systems is particularly amenable to investigation using Raman scattering techniques, since the coupled CDW-lattice excitations can be easily observed in the mixed crystals.

The present paper reports the results of Raman scattering measurements on the mixed-crystal system $1T$-$TaS_{2-x}Se_x$. The experimental apparatus and techniques used and the results obtained are presented in Sec. II. In Sec. III, group-theoretical arguments and a simple lattice-dynamical model are used to discuss the evolution of the CDW-induced modes in the pure crystals. It will be seen that a strong interaction between LA and TA phonons at the distortion wave vector likely gives rise to additional strongly coupled CDW-lattice excitations. Also in Sec. III, the concentration dependences of the CDW-lattice modes are discussed in terms of an effective oscillator model. It will be seen that these excitations have remarkably simple concentration dependences, with the CDW contributions to the mode energies being essentially independent of concentration.

II. EXPERIMENT AND RESULTS

The $1T$-$TaS_{2-x}Se_x$ crystals were grown by iodine vapor phase transport as described in Ref. 10,

 © 1981 The American Physical Society

and were kindly supplied by F.J. Di Salvo. Typical sample dimensions were $5 \times 5 \times 0.1$ mm^3. The samples were glued to a copper substrate using G.E. 7031 varnish and cleaved with Scotch tape immediately prior to mounting in a conduction-tail liquid-nitrogen cryostat. This procedure resulted in excellent mirrorlike surfaces very suitable for Raman scattering measurements. The Raman Scattering apparatus consisted of a Coherent Radiation model 52 argon-ion laser, a Spex model 1401 double monochromator, and photon counting electronics. Instrumental resolution was typically 3 cm^{-1}. The Raman measurements were made using a pseudo-Brewster angle scattering geometry, with two cylindrical lenses (rotated by 90°) being used to focus the incident laser beam on the sample. The spectrometer was advanced in 0.5-cm^{-1} increments and the data were recorded digitally for each spectrometer setting. Argon and mercury calibration lines were included in each spectrum.

Figures 1 and 2 show the Raman spectra of $1T$-$TaS_{2-x}Se_x$ for several values of x. The data were obtained using the 488-nm argon laser line, with 45 mW of incident power. The scattered light was unanalyzed, so that modes of all Raman-active symmetries could be observed. The nominal sample temperature was 90 K, and Stokes-anti-Stokes measurements showed that the local sample temperature differed from this value by no more than ± 5 K. This is of some importance, since several of the observed Raman peaks are rather strongly temperature dependent.[7] Since the sample temperatures were all the same, the measured frequency shifts are indeed due to differences in sample composition.

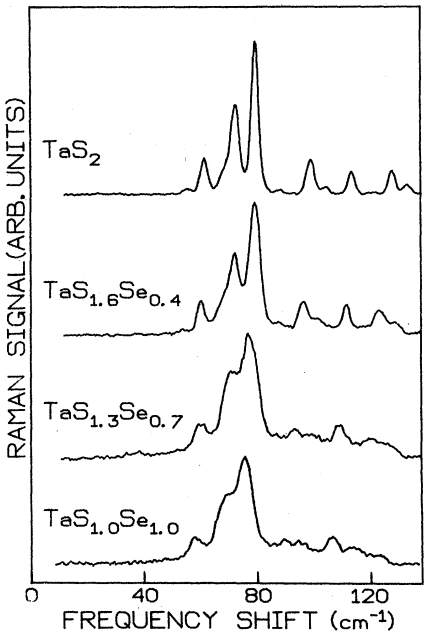

FIG. 1. Unanalyzed Raman spectra of $1T$-$TaS_{2-x}Se_x$ for $x = 0.0$, 0.4, 0.7, and 1.0. The sample temperature was 90 K for each spectrum.

The published Raman and infrared data[5-8] on the pure compounds TaS_2 show considerable structure above 150 cm^{-1}. The corresponding high-frequency lines in the mixed-crystal spectra were very weak and broad. Separate lines could be distinguished only near $x = 0$ and 2. Thus the high-frequency regions of the Raman spectra have not been included in Figs. 1 and 2.

The Raman spectra of Figs. 1 and 2 show several overlapping peaks, with the problem being especially severe for concentrations near $x = 1$. Polarized Raman scans were used to help trace the individual peaks over the whole concentration range. All modes were found to retain the same polarization behavior for all concentrations.[11] The observed mode frequencies are summarized in Table I.

III. DISCUSSION

A. Pure-crystal results

Let us first consider superlattice formation and its consequences on the lattice dynamics of the pure $1T$-structure compounds. In the absence of a CDW, the crystalline structure would be described by space group D_{3d}^3, with one formula unit per unit cell. Group-theoretical considerations predict $\vec{k} = 0$ optic phonons which transform as the $A_{1g} + E_g + A_{2u} + E_u$ irreducible representations of the D_{3d} point group. However, the crystalline unit cell is substantially larger when the crystal is in the commensurate CDW state. Scruby *et al.*[2] and Moncton *et al.*[3] have shown that the commensurate-state crystal is triclinic with 39 atoms per unit cell. In the approximation that the CDW-induced lattice distortions and force-constant changes are small, the coupled CDW-lattice excitations of the commensurate-state crystal can be derived from the undistorted crystal phonon dispersion curves by folding the phonons at the distortion wave vectors back to the Brillouin-zone center. As will be seen later in this section, such an approximation is rather poor, but is does serve as a useful starting point for a discussion of the coupled CDW-lattice excitations.

In what follows, phonon dispersion curves for the *undistorted* $1T$-TaS_2 crystal are calculated using a simple nearest-neighbor, central force-constant model. The resulting dispersion curves are then used to illustrate how the coupled CDW-lattice excitations arise.

TABLE I. Raman frequencies in $1T$-$TaS_{2-x}Se_x$. All frequencies are in cm^{-1}.

x ⟶	0.0	0.4	0.7	1.0	1.5	1.75	2.0
ν (cm^{-1}) ↓	55.4						
	61.6	60.4	59.8	57.9	55.0	53.6	52.9
	67.6	67.5			62.4	61.1	60.2
	72.7	72.3	70.8	69.8	67.0	65.6	63.8
	79.7	79.4	76.5	75.2	73.0	72.8	70.6
	88.5						
	99.1	96.6	92.9	89.8	84.0	81.8	79.8
	104.8	102.2	99.4	95.9	90.4	87.3	84.3
	114.0	111.6	107.9	105.4	101.5	100.2	97.1
	121.4						
	127.9	123.2	119.0	114.0	106.8	104.7	101.0
	133.2	129.4	125.9	123.8	115.5	112.7	108.6

Fig. 3 shows a $(11\bar{2}0)$ section of the undistorted-state structure. The three force constants α, β, and γ used in the lattice-dynamical calculation are indicated. The basal-plane phonon dispersion curves for *one layer* of the crystal were calculated, and the following expressions for the zone-center optic phonons were obtained:

$$\omega^2(A_{1g}) = \frac{3}{M_c}\left(3\frac{\beta}{7}+\frac{3\gamma}{2}\right), \quad \omega^2(A_{2u}) = \frac{18\beta}{7\mu},$$
$$\omega^2(E_g) = \frac{3}{2M_c}\left(4\frac{\beta}{7}+\frac{\gamma}{2}\right), \quad \omega^2(E_u) = \frac{12\beta}{7\mu}, \tag{1}$$

where M_c is the mass of the chalcogen and μ is the reduced mass. These results are very similar to those of Bromley,[12] who carried out a one-layer lattice-dynamical calculation for the $2H$-structure polytypes.

Equations (1) show that the force constants β and γ can be determined by fitting to the undistorted-state zone-center A_{1g} and E_g phonon frequencies. However, since a CDW is always present in these crystals, several Raman peaks occur in the frequency region appropriate for these phonons. Thus, the fitting procedure introduces some uncertainty. From the published Raman data, reasonable assignments for the undistorted-state Raman-active phonon frequencies are $\omega(A_{1g}) = 385\ cm^{-1}$ and $\omega(E_g) = 240\ cm^{-1}$. With these choices, the force constants β and γ for TaS_2 are calculated to be

$$\beta = 9.72\times10^4\ \text{dyn/cm},$$
$$\gamma = 3.48\times10^4\ \text{dyn/cm}, \tag{2}$$
$$\alpha = 3.48\times10^4\ \text{dyn/cm}.$$

Since α does not appear in the expressions for the zone-center phonon frequencies, it was estimated by comparison with the observed Raman spectra and by comparison with calculations for other layered compounds.[12-14] The calculated sound velocities are about 15% higher than those

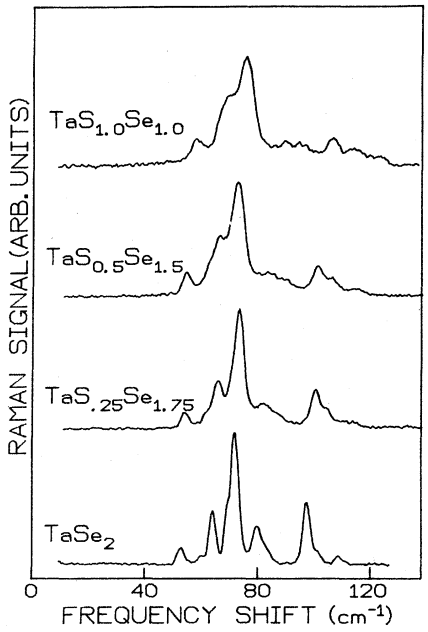

FIG. 2. Unanalyzed Raman spectra of $1T$-$TaS_{2-x}Se_x$ for $x = 1.0$, 1.5, 1.75, and 2.0. The sample temperature was 90 K for each spectrum.

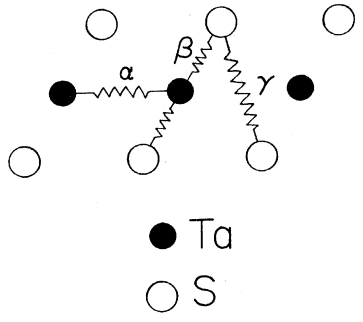

FIG. 3. A $(11\bar{2}0)$ section of the $1T$-polytype crystal structure. The force constants α, β, and γ used in the lattice-dynamical calculation are indicated.

recently measured by Ziebeck *et al.*[15]

Figure 4 shows one layer of the reciprocal lattice of $1T$-TaS_2, after Moncton *et al.*[3] The circled points are those that describe the undistorted crystal. The additional (uncircled) points must be included when the crystal is in the commensurate CDW state. The in-plane components of the distortion wave vectors $\vec{q}_1$, $\vec{q}_2$, and $\vec{q}_3$ are also shown. The hexagon is the undistorted-crystal Brillouin zone, and the numbered points inside it are those that transform to $\vec{k}=0$ when the commensurate-state superlattice forms. It is easily seen that these numbered points are equivalent to the numbered reciprocal-lattice points along the line between A and B in Fig. 4. It is, further, easily seen that the points numbered 2, 4, 5, 10, 11, and 13 are equivalent since they are described by wave vectors $\pm\vec{q}_i$, and that points 3, 6, 7, 8, 9, and 12 are equivalent, since they correspond to wave vectors $\pm(\vec{q}_i-\vec{q}_j)$.

Figure 5 shows the phonon frequencies calculated for $1T$-TaS_2 at the numbered reciprocal-lattice points along the line joining A and B in Fig. 4. The vertical dashed lines indicate the wave vectors of the distorted-state reciprocal-lattice points. The solid curves are guides to the eye. The graph in Fig. 5 has been extended only to the midpoint between A and B, since the dispersion curves must be symmetric about that point. In the limit of weak CDW-lattice coupling, and assuming the correctness of the lattice-dynamical model, the frequencies of the open circles in Fig. 5 should be similar to the observed mode frequencies of TaS_2 in the commensurate CDW state. The short horizontal lines along the right border show the observed Raman frequencies. The near-quantitative agreement between the observed and calculated frequencies shows that the values used for the force constants are reasonable. In particular, the model calculation reproduces the gap between the acoustic and optic branches fairly well.

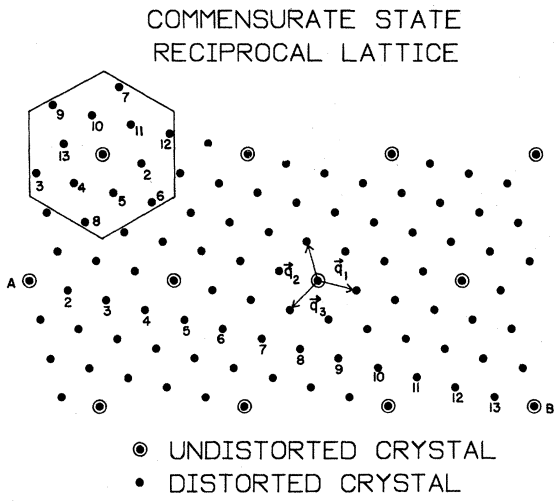

FIG. 4. Reciprocal lattice of $1T$-TaS_2. The circled points alone are appropriate for the undistorted crystal. The uncircled points must be added to describe the commensurate-state crystal. The in-plane components of the distortion wave vectors $\vec{q}_1$, $\vec{q}_2$, and $\vec{q}_3$ are indicated.

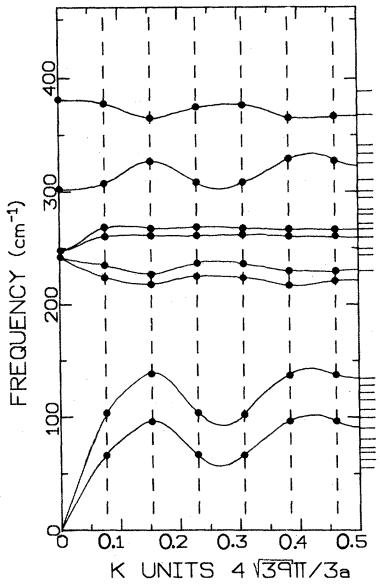

FIG. 5. Calculated phonon dispersion curves for undistorted $1T$-TaS_2 along the direction A–B shown in Fig. 4. The vertical dashed lines indicate the wave vectors that are transformed to the zone center at the transition to the commensurate CDW state.

From the preceding discussion, it is apparent that each branch of the undistorted crystal dispersion curves should give rise to twelve additional optic phonons in the commensurate-state crystal. However, not all of these modes are necessarily Raman active. The space group of the commensurate-state crystal has not yet been determined, but only two possibilities, C_1^1 and C_i^1, exist. Space group C_i^1 has a center of inversion, while C_1^1 does not. If the appropriate space group is C_i^1 then the infrared-active and Raman-active modes will be mutually exclusive. Table II lists the observed Raman and infrared (after Ref. 9) frequencies. Although some of the Raman modes have no corresponding infrared mode, and vice versa, there is correspondence, within experimental uncertainty, for most of the modes. This may indicate that the space group of TaS_2 in the commensurate state is C_1^1, but this conclusion is tempered somewhat by the fact that many near degeneracies are expected. Thirty-six optic

modes should be present in the low-frequency Raman and infrared spectra (twelve modes from each of the three acoustic branches), whereas only 14 distinct modes have been observed (see Table II).

The diffraction results of Scruby *et al.*[2] show that the CDW-induced distortions are mostly longitudinal in the basal plane, indicating that the CDW couples most strongly to the longitudinal-acoustic-phonon branch. This suggests that the strongest features in the pure-crystal Raman spectra should also arise from the undistorted-state longitudinal-acoustic-phonon branch, as discussed by Duffey *et al.*[7] However, CDW-induced modes arising from the undistorted-crystal transverse-acoustic branches cannot be ruled out. This is especially apparent in view of the inelastic neutron scattering results of Ziebeck *et al.*[15] They measured the acoustic phonon dispersion curves of $1T$-TaS_2 in the intermediate incommensurate CDW state (at room temperature), and found a strong Kohn anomaly at the CDW distortion wave vector. Their results for $\vec{k} \parallel [100]$ show that the Kohn-anomaly minimum in the LA branch occurs at 50 cm^{-1}, and further that the TA branch (atomic motions parallel to the c axis) couples strongly with the LA branch at the distortion wave vector. Thus contributions to the observed Raman spectra from the TA branches cannot be ignored.

It is readily apparent from Fig. 5 that in the limit of a small CDW-lattice interaction, the distorted-state $\vec{k}=0$ modes arising from each branch of the undistorted-crystal dispersion curves should occur in two groups of six nearly degenerate modes, one group being derived from the wave vectors $\pm\vec{q}_i$, and the other group coming from wave vectors $\pm(\vec{q}_i - \vec{q}_j)$. However, the low-frequency modes observed in the Raman and infrared experiments cannot be readily separated into groups of six modes. This may in part be due to the LA-TA mixing discussed above, but it also indicates that the CDW contributions to the mode energies are quite substantial. Direct evidence for this is obtained by comparing the observed Raman spectra with the inelastic neutron scattering results. Although the Kohn-anomaly minimum is at 50 cm^{-1} in TaS_2, all of the observed Raman lines lie above this, with the most intense mode being at 80 cm^{-1}. This shows that the CDW contributions are on the order of the mode energies themselves, and it emphasizes the need for a proper microscopic treatment of the CDW-lattice interaction.

Several investigators have presented theoretical descriptions of CDW-lattice excitations. Lee, Rice, and Anderson[16] developed a microscopic theory of such modes in the one-dimensional case. Rice[17] has presented a phenomenological theory of the collective excitations and applied it to the triple CDW case as is appropriate for the layered compounds. McMillan and co-workers have, in a series of papers[8,18-20], developed both Landau and microscopic models of CDW-lattice excitations in the layered compounds. In particular, they have treated the CDW-induced excitations observed by Holy *et al.* with considerable success. Their approach was to write down a potential-energy function including both lattice and electronic contributions and then to solve for the excitation spectrum with the amplitudes and phases of the three equivalent CDW's as the dynamical variables. This approach assumes a linear coupling between the CDW amplitude or phase and the concomitant lattice distortion.

McMillan's model predicts twelve coupled CDW-lattice excitations for $2H$-$TaSe_2$. Only six such excitations are predicted for $1T$-TaS_2 in the commensurate phase, since there is only one layer per unit cell (there are thus only three amplitude degrees of freedom and three phase degrees of freedom). However, this approach is not likely to result in quantitative agreement for $1T$-TaS_2 in view of the strong coupling between the LA and TA phonon branches observed in neutron scattering. This coupling apparently leads to more than six strongly coupled CDW-lattice excitations, as is evidenced by the large number of Raman and infrared modes observed at low frequencies. Thus it would appear that fairly complex models will have to be used to explain the details of the experimental results on $1T$-TaS_2 and $TaSe_2$.

B. Mixed-crystal Raman spectra

Although the observed Raman spectra of pure TaS_2 and $TaSe_2$ have not been explained in detail, a fairly consistent picture of the origins of the coupled CDW-lattice excitations has emerged. The question remains as to how this picture must be modified when the $TaS_{2-x}Se_x$ mixed-crystal results are considered. As was seen in Figs. 1 and 2, the mode frequencies in $TaS_{2-x}Se_x$ all decrease as x is increased from 0 to 2. Figure 6 shows the frequencies plotted as a function of x. The solid lines are guides to the eye. The modes at 55.4, 88.5, and 121.4 cm^{-1} in pure TaS_2 could not be observed for other values of x, apparently because of concentration-induced frequency shifts and broadenings. Each of these modes has a small Raman intensity and is close in frequency to a much stronger peak. The corresponding modes in $TaSe_2$ were not observed, even in high-resolution scans, presumably because

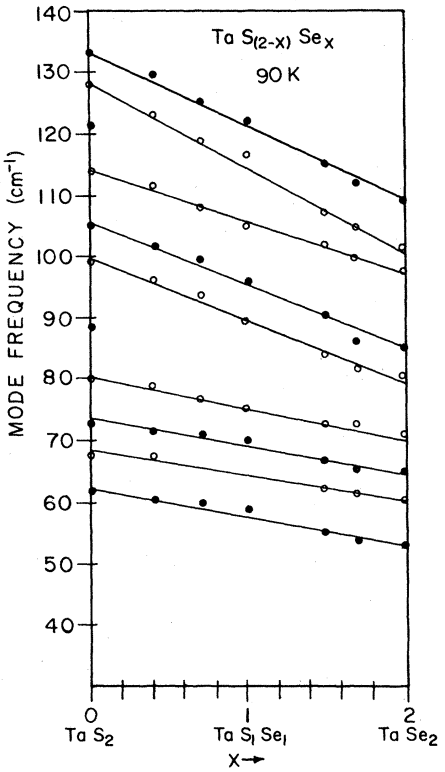

FIG. 6. Concentration dependence of the mode frequencies in $1T$-$TaS_{2-x}Se_x$. The empty and solid circles are the experimental points, and the lines are guides to the eye.

they overlap with nearby strong peaks.

It should be noted that the observed modes remain well defined even near $x=1$, where disorder-induced effects should be most prominent. Figure 7 shows the linewidths (full widths at half maximum) for two of the modes. Although some broadening does occur for the intermediate concentrations, each mode can be treated as a well defined oscillator. Since the modes can also be followed over the whole concentration range, this suggests that each mode can be considered as a simple harmonic oscillator whose character changes very little with concentration. If so, the mode frequencies at concentration x can be written

$$\omega_i(x)=\left(\frac{k_i(x)}{M_i(x)}\right)^{1/2}, \tag{3}$$

where $k_i(x)$ and $M_i(x)$ are the effective force constant and effective mass, respectively, of the ith mode. In principle, both $k_i(x)$ and $M_i(x)$ can be strongly concentration dependent. Let us first consider the concentration dependence of the oscillator mass. Since the observed modes are apparently derived from the undistorted-state longitudinal-acoustic phonons, one might

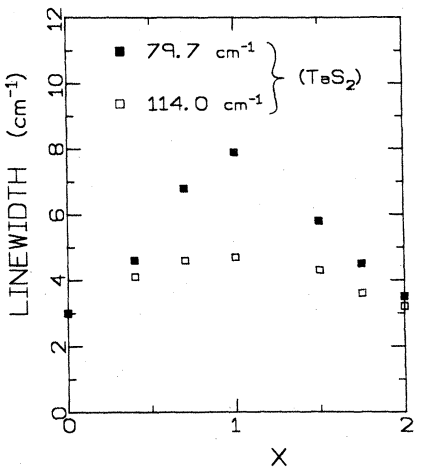

FIG. 7. Full widths at half maximum as a function of Se concentration for the 79.7- and 114.0-cm^{-1} lines in pure $1T$-TaS_2.

expect the oscillator mass to be approximately equal to the total mass of the undistorted unit cell, so that

$$M_i(x)=M_{Ta}+2M_S+(M_{Se}-M_S)x \quad \text{(total mass)}, \tag{4}$$

where M_{Ta}, M_S, and M_{Se} are the masses of the tantalum, sulfur, and selenium ions, respectively.

It should be noted that the above expression is essentially a "virtual-crystal"[21] approximation for the mass of the ith mode. Depending on the atomic motions for the modes, the concentration dependence of the oscillator mass could be stronger or weaker than this. To set some limits we consider other possible effective masses, including a dependence on the reduced mass, a dependence only on the mass of the chalcogens, or a dependence only on the Ta ion mass. The concentration-dependent oscillator masses for these cases are easily seen to be

$$M_i(x)=\frac{M_{Ta}[2M_S+(M_{Se}-M_S)x]}{M_{Ta}+2M_S+(M_{Se}-M_S)x} \quad \text{(reduced mass)}, \tag{5}$$

$$M_i(x)=2M_S+(M_{Se}-M_S)x \quad \text{(chalcogen mass)}, \tag{6}$$

$$M_i(x)=M_{Ta} \quad \text{(tantalum mass)}. \tag{7}$$

If the force-constant changes with concentration are assumed to be small, then the ratio of the ith-mode frequency at concentration x to that at concentration 0 is given by

$$\frac{\omega_i(x)}{\omega_i(0)}=\left(\frac{M_i(0)}{M_i(x)}\right)^{1/2}. \tag{8}$$

The solid circles in Fig. 8 show $\omega_i(x)$ plotted as a function of $\omega_i(0)$ for $x=1.5$. The straight lines are the calculated curves for each of the preceding mass dependences. As can be seen, the

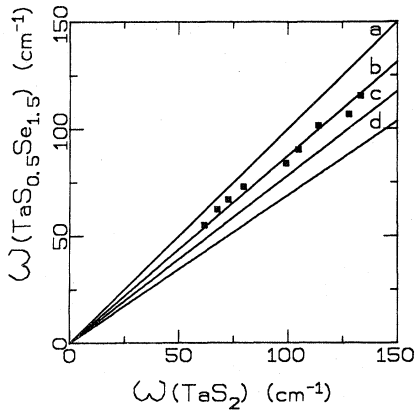

FIG. 8. Mode frequencies for $1T$-$TaS_{0.5}Se_{1.5}$ plotted versus the corresponding mode frequencies in pure $1T$-TaS_2. The squares are the experimental points. The straight lines are the predicted mass dependences. Curve *a*: chalcogen mass dependence. Curve *b*: total mass dependence. Curve *c*: reduced mass dependence. Curve *d*: tantalum mass dependence.

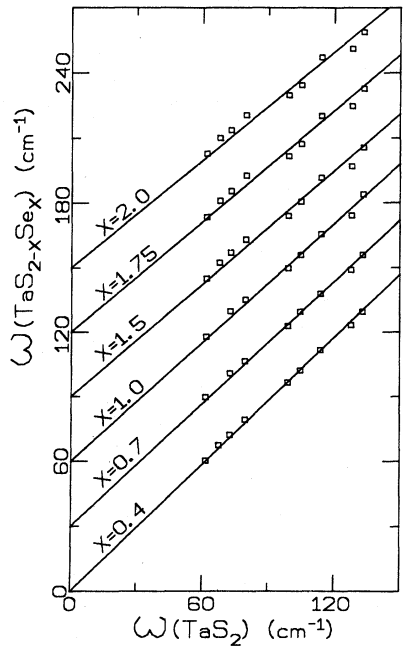

FIG. 9. Mode frequencies for $1T$-$TaS_{2-x}Se_x$ plotted versus the corresponding mode frequencies in pure $1T$-TaS_2. The squares are the experimental points, and the straight lines are least-squares fits constrained to pass through the origin. The origins of successive sets of data have been shifted upwards by 30 cm^{-1} for clarity.

curve obtained from the total mass dependence [curve (b)] fits the experimental results best.

Figure 9 shows plots similar to that of Fig. 8 for all values of x investigated here. The origins of successive sets of data have been shifted upwards by 30 cm^{-1} for clarity. The straight lines are least-squares fits constrained to pass through the origin. The slopes of these lines are compared with the slopes in Table II predicted by Eqs. (4) and (8); the oscillator frequency is assumed to depend on the total molecular mass. In each case, the calculated and experimentally determined slopes agree to within the uncertainty in the fit.

The scatter of the experimental points about the fitted curves in Fig. 9 is considerably greater than experimental error. The four lowest-frequency modes and the mode at 114 cm^{-1} in pure TaS_2 consistently lie above the fitted curves, while the four remaining modes consistently lie below the fitted curves. These deviations from the total mass scaling behavior may reflect either a different effective-mass dependence from that which was assumed, or a dependence of the effective force constants on concentration. However, these effects seem to be quite small, which indicates that the CDW contributions to the mode energies are essentially independent of concentration.

TABLE II. Experimental and predicted slopes for the data in Fig. 9. $M(x)$ is the total molecular mass of Eq. (4).

x	$\left(\frac{M(0)}{M(x)}\right)^{1/2}$	Measured slope
0.4	0.964	0.98
0.7	0.939	0.95
1.0	0.916	0.92
1.5	0.881	0.87
1.75	0.866	0.85
2.0	0.850	0.82

In a very recent paper, Inglesfield[22] has investigated the electronic structure of $1T$-TaS_2 using hybridized orbitals. He found that the conduction electrons responsible for the CDW phase transition arise from nonbonding orbitals on the transition-metal atoms. He also carried out a tight-binding calculation of the conduction-electron contribution to the phonon-dynamical matrix. His results indicate that this contribution is strongly negative, and in fact that it dominates the short range and electrostatic contributions to the dynamical matrix over a large range of k space near the distortion wave vector. This suggests that the distortion wave vector is indeed determined by Fermi-surface effects. From the d-electron bandwidths, Inglesfield estimated that the sizes of the electronic contribution to the dynamical matrix are quite similar in $1T$-TaS_2 and $1T$-$TaSe_2$. This is consistent with our re-

sult that the observed CDW-induced modes scale in a simple manner with the atomic masses.

IV. SUMMARY

We have reported the results of Raman scattering measurements on the mixed-crystal system $1T$-$TaS_{2-x}Se_x$ in the commensurate charge-density-wave state. For pure TaS_2, many low-frequency CDW-induced modes were observed, some of which likely arise because of a strong LA-TA phonon interaction at the distortion wave vector. It was possible to follow most of the CDW-induced modes over the whole concentration range. The concentration dependences of the mode frequencies were analyzed using an effective oscillator model in which the oscillator mass is the total mass of the $TaS_{2-x}Se_x$ molecule. These results indicate that the CDW contributions to the mode effective force constants are essentially independent of concentration.

ACKNOWLEDGMENTS

We are very grateful to F. J. DiSalvo for supplying us with excellent mixed-crystal samples, and we are pleased to acknowledge B. P. Clayman for very helpful discussions of his infrared results on TaS_2 and $TaSe_2$. This work was supported by the National Science Foundation under Grant No. DMR77-10217.

---

*Present Address: Hughes Aircraft Co., Developmental Products Laboratory, Centinela & Teale, Culver City, CA 90230.

[1]J. A. Wilson, F. J. DiSalvo, and S. Mahajan, Adv. Phys. 24, 117 (1975).
[2]C. B. Scruby, P. M. Williams, and G. S. Parry, Philos. Mag. 31, 255 (1975).
[3]D. E. Moncton, F. J. DiSalvo, J. D. Axe, L. J. Sham, and B. R. Patton, Phys. Rev. B 14, 3432 (1976).
[4]G. K. Wertheim, F. J. DiSalvo, and S. Chiang, Phys. Rev. B 13, 5476 (1967). See also Phys. Lett. 54A, 304 (1975).
[5]J. E. Smith, J. C. Tsang, and M. W. Shafer, Solid State Commun. 19, 283 (1976).
[6]J. C. Tsang, J. E. Smith, M. W. Shafer, and S. F. Meyer, Phys. Rev. B 16, 4239 (1977).
[7]J. R. Duffey, R. D. Kirby, and R. V. Coleman, Solid State Commun. 20, 617 (1976).
[8]J. A. Holy, Ph.D. thesis, University of Illinois at Champaign-Urbana, 1977 (unpublished).
[9]D. R. Karecki and B. P. Clayman, Solid State Commun. 19, 479 (1976). See also, Phys. Rev. B 19, 6367 (1979).
[10]F. J. DiSalvo, J. A. Wilson, B. G. Bagley, and J. V. Waszczak, Phys. Rev. B 12, 2220 (1975).
[11]See Ref. 7 for the polarization dependences of the observed modes.
[12]R. A. Bromley, Philos. Mag. 23, 1417 (1971).
[13]J. L. Verble and T. J. Wieting, Phys. Rev. Lett. 25, 362 (1970).
[14]J. L. Verble, T. J. Wieting, and P. R. Reed, Solid State Commun. 11, 941 (1974).
[15]K. Ziebeck, B. Dorner, W. G. Stirling, and R. Scholhorn, J. Phys. F 7, 1139 (1977).
[16]P. A. Lee, T. M. Rice, and P. W. Anderson, Solid State Commun. 14, 703 (1974).
[17]T. M. Rice, Solid State Commun. 17, 1055 (1975).
[18]W. L. McMillan, Phys. Rev. B 12, 1187 (1975).
[19]W. L. McMillan, Phys. Rev. B 16, 643 (1977).
[20]W. L. McMillan, Phys. Rev. B 16, 4655 (1977).
[21]A. S. Barker and A. J. Sievers, Rev. Mod. Phys. 47 (Suppl. 2), S1 (1975).
[22]J. E. Inglesfield, J. Phys. C 13, 17 (1980).